PERGAMON

International Journal of Heat and Mass Transfer 42 (1999) 437–454

International Journal of HEAT and MASS TRANSFER

Double diffusive convection in dual-permeability, dual-porosity porous media

M. Z. Saghir[a,*], M. R. Islam[b]

[a] *Department of Mechanical Engineering*;
[b] *Department of Chemical and Petroleum Engineering, U.A.E. University, P.O. Box 17555, Al-Ain, U.A.E.*

Received 13 February 1998; in final form 21 May 1998

Abstract

A numerical study, using a finite element formulation, is conducted in order to study double diffusive phenomena in porous media. The Brinkman model is used as the momentum balance equation and is solved simultaneously with mass and energy balance equations in a two-dimensional domain. Special emphasis is given to the study of double diffusive phenomena in a layered porous bed with contrasting permeabilities. The extent of cross flow and its role in determining the shape, as well as the propagation, of the intruding plume are studied for a range of both thermal and solutal parameters. The study is completed for a wide range of permeability contrasts.

1. Introduction

Even though double diffusive convention is present in almost all naturally occurring porous media, it remains one of the most elusive topics in porous media studies. Heat and mass transfer driven convection in porous media has a large number of applications in the disposal of waste material, groundwater contamination, chemical transport in packed-bed reactors,and others. One can cite the problem of heat and mass transfer during acidization of a wellbore, production of hot water in a geothermal well (leading to significant thermal and solutal gradient) and liquid fuel storage in a salt dome, as some of the examples of relevant engineering problems. Very few studies have addressed double diffusive phenomena in porous media and have assumed the transport medium to be homogeneous and isotropic. The problem of double diffusion in porous media is addressed in this paper when the porous medium is layered with contrasting permeabilities.

1.1. Double diffusive phenomena

When heat and mass transfer takes place within a fluid layer, temperature and concentration gradients create a combined convection mode. This phenomenon is called double diffusive convection. Even though evidence indicates that double diffusive processes were observed centuries ago [1], the role of double diffusion on the motion of an intruding fluid remains among some of the most elusive topics of fluid mechanics [2].

One of the landmark studies of double diffusive convection in an open channel was conducted by Maxworthy [3]. In order to elucidate some of the incipient features of double diffusive phenomena, he studied the intrusion of a sugar solution into a salt solution. The use of two different diffusivity rates (diffusivity of sugar being less than that of salt) enabled him to measure the spreading rates of the two-dimensional double diffusive intrusion. He found that the transfer of mass and momentum across the sugar/salt interface dominates the motion of intrusion. This experimental work of Maxworthy drew significant attention in the literature and was later mathematically modeled by [1] and Saghir et al. [4].

Even though the petroleum engineering literature is rich in observing double diffusive phenomena in multi-

* Corresponding author. Tel: 00 971 3 5051 569; Fax: 00 97 13 632 382; E-mail: saghirz@omar.uaeu.ac.ae

0017–9310/98 $19.00
PII: S0017–9310(98)00183–5

phase flow systems, the isolated observation of double diffusion in a single phase system is relatively new [5]. Manole and Nield [6] studied natural convection in a horizontal porous layer induced by inclined thermal and solutal gradients with horizontal mass flow. A theoretical examination was made for convection induced by applied thermal and solutal coplanar gradients inclined to the vertical direction. Results indicated that the role of the horizontal gradient switches from stabilizing to destabilizing as the magnitude of the gradient increases.

Chen and Chen [7] studied two-dimensional double diffusive fingering convection in a horizontal porous medium in which periodic conditions were subscribed. By solving the problem for different thermal Rayleigh numbers, they found three different types of critical solutal Rayleigh numbers. The first deals with the critical value for the onset of steady fingering, the second for the transition from steady convection to periodic convection and the third with the transition from periodic convection to unsteady convection.

Zongqin and Bejan [8] investigated the horizontal spreading of thermal and chemical deposits in a porous medium. They found solutions to the problem both analytically and numerically. In particular, their research emphasized buoyancy-driven horizontal spreading of heat and chemical species through a fluid-saturated porous medium. The buoyancy effect was found to be due to both thermal and solutal gradients. It was shown that when the flow is driven primarily by temperature gradients, the thermal equilibrium could take place either by convection or by diffusion.

1.2. Heterogeneity in porous media

The study of double diffusive convection in porous media is relatively new [9–11], and has been devoted to homogeneous, isotropic porous media only. Even though naturally occurring porous media are known to be heterogeneous, both microscopically and macroscopically, the assumption of homogeneity is usually invoked to simplify the problem. A simplified model is helpful for resolving effects that are not fully coupled with heterogeneity. However, due to this simplification, the role of heterogeneity, random or ordered, remains unexplored in the areas of double diffusive convection in porous media.

Published studies in petroleum engineering show that natural porous media can exhibit heterogeneities in various scales: small, medium and large [12–13]. Most studies in petroleum engineering, however, are aimed at determining pseudo functions for scaling up laboratory results to field scales with the aid of a numerical simulator. Ahmadi et al. [14] have recently reviewed various approaches proposed to solve multiphase flow in a layered porous bed. Even though it has been known for some time that multiphase flow is significantly affected by large-scale heterogeneities [15], the significance of small-scale heterogeneities has been discovered only recently [16–17].

The study of the effect of heterogeneity on fluid convection should start with the investigation of cross flow in a two-layer system [18–19]. Most of these studies have concentrated on two-phase flow without any chemical transport [20–21]. These researchers studied the competition of non-linear processes involving capillary, gravity and viscous forces. For two-phase flow, viscosity and density ratios, rock/fluid properties and flow rate govern all these forces. For most cases, geometrical properties have been found to influence the complex interplay among various forces [22–23]. More recently, Eilertsen et al. [18] studied two-phase flow in an inclined cross-layered porous bed. They demonstrated the importance of both geometry and layered cross flow on the overall flow mechanism.

Few studies have been reported on the role of heterogeneities on solutal convection. Tchelepi and Orr [24] studied the role of heterogeneity in miscible displacement processes. Their study was limited to observing the growth of a viscous finger that might have been triggered by heterogeneity in porous media. In general, numerical study of the propagation of viscous fingers remains in its infancy [25]. Studies are even more rare when it comes to investigating double diffusive phenomena in porous media, especially in the presence of macroscopic or microscopic heterogeneity.

This paper is aimed at observing double diffusive phenomena in a layered porous bed with contrasting permeabilities. The extent of cross flow and its role in determining the shape of the intruding plume are studied for a range of thermal and solutal parameters. The study is completed for a wide range of permeability contrasts.

2. Governing equations and numerical procedure

The Brinkman equation was used as the momentum balance equation. This equation along with energy and solutal equations were solved numerically using the finite element technique. Following is a list of governing equations solved in this study.

2.1. Governing equations and boundary conditions

The momentum balance equation was represented by the Brinkman equation. In the x direction, this equation is written as follows:

$$\frac{\rho}{\phi}\frac{\partial u}{\partial t}+\left[\frac{\mu}{\kappa}\right]u=-\frac{\partial p}{\partial x}+\mu_e\left[\frac{\partial^2 u}{\partial x^2}+\frac{\partial^2 u}{\partial y^2}\right], \tag{1}$$

whereas in the y direction, the equation is written as:

$$\frac{\rho}{\phi}\frac{\partial v}{\partial t}+\left[\frac{\mu}{\kappa}\right]v=-\frac{\partial p}{\partial y}+\mu_{\mathrm{e}}\left[\frac{\partial^2 v}{\partial x^2}+\frac{\partial^2 v}{\partial y^2}\right]-\rho g[\beta_{\mathrm{T}}(T-T_o)-\beta_{\mathrm{C}}(c-c_o)]. \quad (2)$$

In the equations above, (u, v) are the velocity components in the x and y directions, respectively. The pressure is denoted by p, the temperature is T, the concentration is c, the density is ρ and the time is denoted by t. The thermal volume expansion is β_T, the solutal volume expansion is denoted by β_C, the viscosity is denoted by μ, the effective viscosity is denoted by μ_{e}, the permeability is denoted by κ, the porosity by ϕ and g is the gravity term. The Brinkman approximation sets the fluid viscosity μ and μ_{e} equal to each other but, in general, they are approximately equal.

The continuity equation is given by the following expression for a two-dimensional system;

$$\left[\frac{\partial u}{\partial x}+\frac{\partial v}{\partial y}\right]=0. \quad (3)$$

The energy balance equation is expressed as follows

$$\rho C_{\mathrm{p}}\left[\frac{\partial T}{\partial t}\right]+(\rho C_{\mathrm{p}})_{\mathrm{f}}\left[u\frac{\partial T}{\partial x}+v\frac{\partial T}{\partial y}\right]=\kappa\left[\frac{\partial^2 T}{\partial x^2}+\frac{\partial^2 T}{\partial y^2}\right]. \quad (4)$$

Along with the energy balance equation, the following constitutive thermal relationships were used

$$\rho C_{\mathrm{p}}=\phi(\rho C_{\mathrm{p}})_{\mathrm{f}}+(1-\phi)(\rho C_{\mathrm{p}})_{\mathrm{s}} \quad (5)$$

$$k=\phi k_{\mathrm{f}}+(1-\phi)k_{\mathrm{s}} \quad (6)$$

where ρC_{p} is the effective product of the density and the specific heat of the system, $(\rho C_{\mathrm{p}})_{\mathrm{f}}$ is the product of the density and the specific heat of the fluid used in the model which is water in our case. In equation (5), $(\rho C_{\mathrm{p}})_{\mathrm{s}}$ is the product of the density and the specific heat of the solid glass bead that constituted the porous medium and the k the effective conductivity of the system. The conductivity of the fluid is denoted by k_{f} and the conductivity of the solid glass bead is denoted by k_{s}.

The mass transfer equation for the solute is written as follows:

$$\left[\phi\frac{\partial c}{\partial t}+u\frac{\partial c}{\partial x}+v\frac{\partial c}{\partial y}\right]=\alpha_{\mathrm{C}}\left[\frac{\partial^2 c}{\partial x^2}+\frac{\partial^2 c}{\partial y^2}\right], \quad (7)$$

where c is the solute concentration and α_{C} is the solutal diffusion coefficient. Equations (1)–(7) were made dimensionless by using the following dimensionless variables:

$$U=\frac{u}{u_o},\quad V=\frac{v}{u_o},\quad X=\frac{x}{L},\quad Y=\frac{y}{L},$$

$$P=\frac{p}{\rho u_0^2},\quad u_o=\sqrt{g\beta_{\mathrm{T}}\Delta TL},\quad \tau=\frac{tu_o}{L},$$

$$\theta=\frac{T-T_o}{\Delta T},\quad C=\frac{c-c_o}{\Delta C} \quad (8)$$

where u_{o} is a reference velocity, ΔT the initial temperature difference, and L is a characteristic length. Another dimensionless parameter, the buoyancy term (N), is defined as the ratio of the salty water density difference to the fresh water density difference. Since the density of the salty water (slower diffusing substance) is written as $\rho_{\mathrm{C}}=\rho(1+\beta_{\mathrm{C}}\Delta C)$ and the density of the fresh water (faster diffusing substance) is written as $\rho_{\mathrm{T}}=\rho(1+\beta_{\mathrm{T}}\Delta T)$, the buoyancy ratio N can be written as

$$N=\frac{\rho_{\mathrm{C}}-\rho}{\rho_{\mathrm{T}}-\rho}=\frac{\beta_{\mathrm{C}}\Delta C}{\beta_{\mathrm{T}}\Delta T}.$$

In this study, a value of $N=1$ was used. Equations (1)–(7) in their dimensionless forms become as follows:

Momentum equation

x-direction

$$\frac{1}{\phi}\left[\frac{\partial U}{\partial \tau}\right]+\left[\frac{\sqrt{Pr}}{\sqrt{Ra_{\mathrm{T}}Da}}\right]U=-\frac{\partial P}{\partial X}+\frac{\sqrt{Ra_{\mathrm{T}}}}{\sqrt{PrDa}}\left[\frac{\partial^2 U}{\partial X^2}+\frac{\partial^2 U}{\partial Y^2}\right] \quad (9)$$

y-direction

$$\frac{1}{\phi}\left[\frac{\partial V}{\partial t}\right]+\left[\frac{\sqrt{Pr}}{\sqrt{Ra_{\mathrm{T}}Da}}\right]V=-\frac{\partial P}{\partial Y}+\frac{\sqrt{Ra_{\mathrm{T}}}}{\sqrt{PrDa}}\left[\frac{\partial^2 V}{\partial X^2}+\frac{\partial^2 V}{\partial Y^2}\right]-[\theta-NC] \quad (10)$$

Continuity equation

$$\frac{\partial U}{\partial X}+\frac{\partial V}{\partial Y}=0 \quad (11)$$

Energy equation

$$\left[G\frac{\partial \theta}{\partial \tau}+U\frac{\partial \theta}{\partial X}+V\frac{\partial \theta}{\partial Y}\right]=\frac{\sqrt{Da}}{\sqrt{Ra_{\mathrm{T}}Pr}}\left[\frac{\partial^2 \theta}{\partial X^2}+\frac{\partial^2 \theta}{\partial Y^2}\right] \quad (12)$$

In the above equations $Da=\kappa/L^2$ is the Darcy number,

$$Ra_{\mathrm{T}}=\frac{g\beta_{\mathrm{T}}\Delta TL\kappa}{\alpha v}$$

is the modified thermal Rayleigh number, and $Pr=v/\alpha$ is the Prandtl number. Also, G is the ratio of the effective product of the density and the specific heat to the fluid product of the density and the specific heat. In particular, using equation 5, this constant becomes:

$$G=\frac{\rho C_{\mathrm{p}}}{(\rho C_{\mathrm{p}})_{\mathrm{f}}}=\phi+\frac{(\rho C_{\mathrm{p}})_{\mathrm{s}}}{(\rho C_{\mathrm{p}})_{\mathrm{f}}}(1-\phi) \quad (13)$$

Mass balance equation

$$\left[\phi\frac{\partial C}{\partial \tau}+U\frac{\partial C}{\partial X}+V\frac{\partial C}{\partial Y}\right]=\frac{\sqrt{NDa}}{\sqrt{Ra_{\mathrm{C}}Sc}}\left[\frac{\partial^2 C}{\partial X^2}+\frac{\partial^2 C}{\partial Y^2}\right] \quad (14)$$

One of the most important parameters in double diffusive phenomena is the Lewis number Le. It is known to be the ratio of the thermal diffusivity to the solutal diffusivity

of the system. Together, the thermal Rayleigh number Ra_T and the solutal Rayleigh number Ra_C are related through the buoyancy term and the Lewis number as $Ra_C = Ra_T . N . Le$, where the Lewis number Le is equal to Sc/Pr. The term $Sc = \nu/\alpha_C$ is the so-called Schmidt number and

$$Ra_C = \frac{g\beta_C \Delta C L \kappa}{\upsilon \alpha_C}$$

is the solutal Rayleigh number.

Figure 1 shows a schematic of the physical setup along with the boundary conditions used in this analysis. It consists of a cavity having a width (W_1) of 0.5 cm and a length (L) of 1 cm enclosed in a cavity of 1 cm width (L_2) and 10 cm length (W_2). Because most petroleum, geothermal, and nuclear waste disposal applications deal with a relatively large aspect ratio, an aspect ratio of 10 is selected for this study. Previous studies indicate that salient features of heat and mass transfer are altered significantly below an aspect ratio of 0.6 [27] and beyond an aspect ratio of 3 [11]. In this study, by selecting an aspect ratio of 10, we have opted to model a scenario that depicts physical phenomena of a system of aspect ratio greater than 3. Such aspect represents all salient features of a petroleum, geothermal, or nuclear waste disposal problem [28]. The 'smaller' porous cavity contains the cold fresh water known as the faster diffusing solution and the larger porous cavity contains the hot salty water known as the slower diffusing solution. The porosity of the two cavities is assumed to be identical and isotropic. As shown in Fig. 1, the upper part of the larger cavity including the smaller cavity has a higher permeability designated by its Darcy number Da_2 whereas the lower cavity has a different permeability designated by its Darcy number Da_1. At a time $t = 0$ seconds, the fresh water is released to the salty porous cavity. The initial temperature and concentration differences, between the salty water and the fresh water, are set equal to unity. The temperature boundary condition dictates that no heat be lost to the environment. Therefore, at all sides of the cavity, zero heat flux or temperature gradient normal to the wall is applied. In addition, zero concentration gradient normal to the cavity wall is prescribed. The velocity at all external walls of the cavity

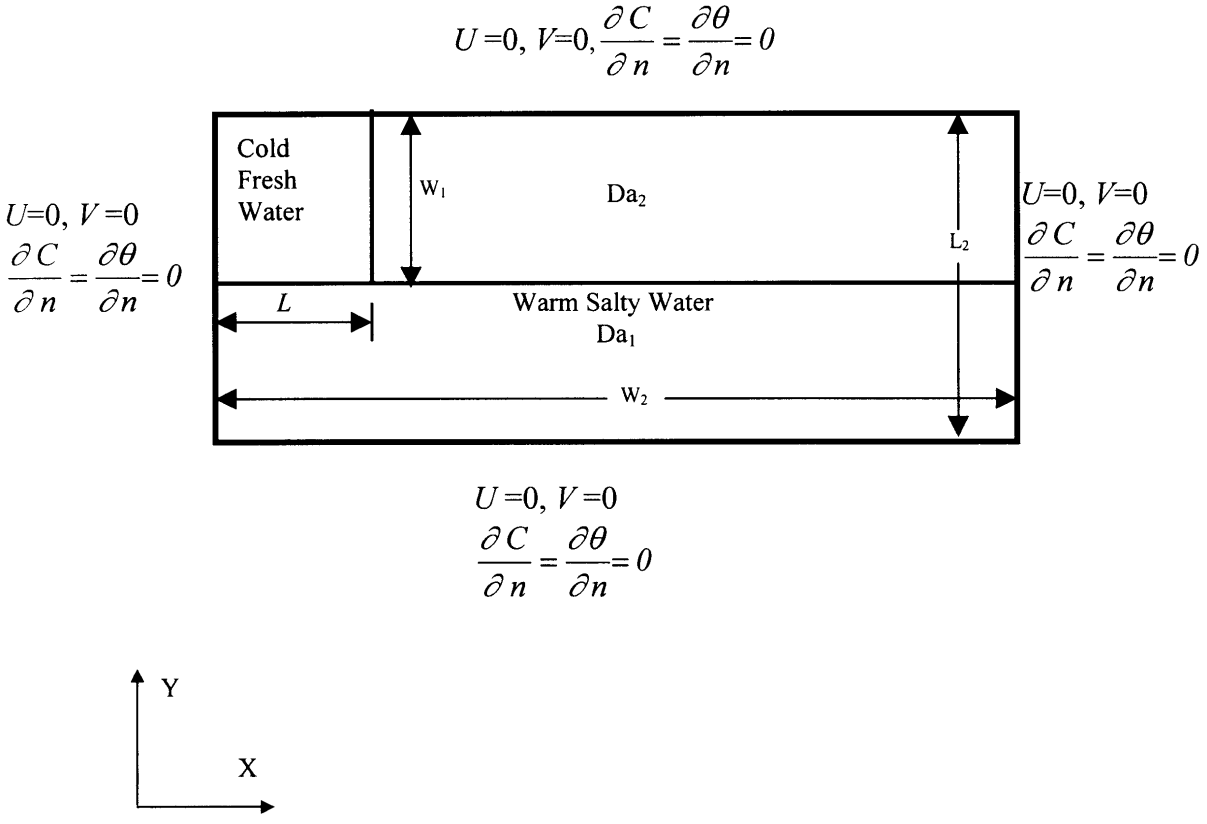

Fig. 1. Schematic of the porous medium.

are assumed to be equal to zero, invoking the conventional no-slip boundary conditions. No other boundary condition is required to solve the problem.

2.2. Finite element formulations

The numerical scheme consisted of solving the non-dimensional equations (9), (10), (11), (12) and (14) using the finite element technique. A quadrilateral element with velocities, concentration and temperature at each node was used in the model. A linear approximation of the pressure using the penalty method was adopted. The transient problem was solved using the segregated method. At each time step, the four equations were solved simultaneously and the criteria for convergence were set on the four unknowns namely the two velocities, the temperature and the concentration. Once all these variables, at two different time steps, reached a difference less than 10^{-4}, the convergence was considered to have been achieved. All numerical solutions reported in this paper were obtained using a uniform grid in which 95 quadrilateral elements covered the horizontal direction and 21 quadrilateral elements covered the vertical direction. The inclusion of more concentrated meshes near the inlet, where the maximum solutal gradient existed, resulted in longer time required for convergence without producing any different result. Such behavior is expected because the solutal gradient is not very steep. In total, 1995 quadrilateral elements were used in the model. Extensive numerical accuracy test showed that the chosen grid is adequate for the model. For further details of the numerical formulation see Saghir et al. [4].

The bead diameter, d, used in our model is 3.25 mm. Using the Kozeny–Carmen relationship [26] and by maintaining the porosity constant and equal to 0.39, the permeability is expressed as follows:

$$\kappa = \frac{d^2}{174.3}\frac{\phi^3}{(1-\phi)^2} \tag{15}$$

This will result in a permeability having a value of $\kappa = 9.7\times10^{-5}$ cm^2. Since the characteristic length used in our model, based on Fig. 1, is $L = 1$ cm, the Darcy number which will be used in this study is $Da_1 = 9.7\times10^{-5}$. The Darcy number Da_2 of the upper cavity will be varied for different permeability contrasts (i.e. ratio $= Da_2/Da_1$). Table 1 illustrates the physical properties of the water and glass beads. Finally the ratio of the thermal diffusivity in both horizontal and vertical directions was assumed to be equal to unity. Table 2 summarizes all the cases to be studied by presenting the non-dimensional terms involved in modeling for $N = 1$. It is worth mentioning that the thermal and solutal Rayleigh numbers in Table 2 are the initial Rayleigh numbers. Once the velocities were computed, the stream function φ was determined using the following well-known relationship,

$$u = \frac{\partial\varphi}{\partial y} \quad \text{and} \quad v = -\frac{\partial\varphi}{\partial x}.$$

Stream function is non-dimensionalized using a reference stream function value given by $\psi_o = Lu_o$.

3. Results and discussion

A series of numerical runs was conducted in order to investigate the role of cross flow between layers. Also, the effects of thermal and solutal parameters were investigated for a selected case. For all cases, the two layers were assumed to have the same thickness. Following is a discussion of various effects observed in this study.

3.1. Effect of permeability contrast

Seven numerical runs were conducted to investigate the extent of cross flow between layers. Permeability contrast values were varied from 0.5 through 100. All other parameters were kept the same. Figure 2 shows the concentration profiles 180 s after the release of cold water for various cases. Even though the water front traveled different distances for different cases, a significant change in the shape of the curve occurs starting from a permeability ratio as high as seven. From this permeability ratio onward, there is a distinct change in the shape of the concentration profile. A more profound change takes place for a permeability ratio of 10 for which all the concentration profiles exhibit distinct optima near the interface between the two-permeability layers. Concentrations trail considerably in the lower-permeability bottom layer. However, as the permeability ratio is increased, the lower leg of the concentration profile keeps pace with the top part, leading to the formation of a finger-like structure. In order to determine the flow pattern, the stream function contours for various cases are plotted in Fig. 3. The existence of permeability discontinuity starts to show for a permeability ratio of 3. The non-uniform cross-flow between layers is more clearly evident for a permeability ratio of 5, and is accentuated for a ratio of 10. Note that the center of the streamlines is formed above, the dividing line of the two permeability layers. Also, most of the convective circulation takes place in the upper portion of the porous layer. As the fluid encounters permeability discontinuity (with more resistance to flow), velocity is reduced leading to the formation of a spread to the streamline contour. Because the amount of total release is the same for all cases, increased circulation takes place in the upper portion of the bed. This pattern accounts for much of the finger-like propagation of the concentration profiles. For a permeability ratio of 50, the center of the vortex remains approximately in the same location, but the streamlines in the lower bed become even more sparse. Most of the

Table 1
Physical properties of the fluid and glass beads

	Density ($g\ cm^{-3}$)	Viscosity ($g\ cm^{-1}\ s^{-1}$)	Conductivity ($cal\ cm^{-1}\ K^{-1}$)	Specific heat ($cal\ s^{-1}\ g^{-1}\ K^{-1}$)
Water	1.000	1.003×10^{-2}	1.443×10^{-3}	1.4386
Glass bead	1.648	—	4.329×10^{-3}	0.1147

Table 2
Non-dimensional parameters used in the porous model

$N=1$	Ra_T	Ra_C	Le
$Da_1=9.7\times10^{-5}$	2	2	
$Da_2=4.85\times10^{-5}$	1	1	
$Da_2=2.91\times10^{-4}$	6	6	1
$Da_2=4.8\times10^{-4}$	10	10	
$Da_2=9.70\times10^{-4}$	20	20	
$Da_2=2.91\times10^{-3}$	60	60	1
	60	6000	100
	1200	1200	1
$Da_2=4.85\times10^{-3}$	100	100	
$Da_2=6.79\times10^{-3}$	140	140	1
$Da_2=9.70\times10^{-3}$	200	200	

convection takes place in the upper bed. The trend of increasing convective strength in the upper bed becomes less pronounced as the permeability ratio is increased further. Even for a permeability ratio of 100, some fluid convection, even though weakened, takes place in the low-permeability lower layer.

Figure 4 show the temperature distribution for various cases. Similar to the previous two plots, the temperature contours are plotted 180 s after the release of cold water. Temperature profiles appear to be the least affected by the permeability variation. They appear to be almost identical for a permeability ratio of up to 10 at which point the vertical isotherms start to become S-shaped near the point of release. Because convection in the lower region is less intense at higher permeability ratio cases, heat conduction becomes the only means of thermal propagation, leaving the lower legs of the isotherms more dispersed. This trend continues with equal vigor for higher permeability ratio cases. However, as the permeability ratio is increased, there is no clear change in the temperature distribution. This temperature distribution is in harmony with the convective rolls that are reported earlier.

In order to observe the propagation of the concentration front as a function of permeability ratios, the intrusion length values are plotted for various permeability contrasts (Fig. 5). The intrusion length is significantly affected by the permeability ratio for up to a value of 30. At lower permeability ratio values, the intrusion length remains insensitive to the permeability ratios. This indicates that the cross-flow between the two layers remains intense and the fluid front does not 'see' any discontinuity in permeability. As long as the permeability contrast is not very sharp, the total cross section of the porous bed contributes to fluid propagation. There is a linear increase in intrusion length for a permeability ratio ranging from 10 through 50. For these cases, any increase in permeability ratios translates into direct decrease in the cross section available to fluid flow. Beyond a permeability ratio of 50, there appears to be a stabilizing effect in place and any further increase in the permeability ratio does not affect the intrusion length to any appreciable degree. At very high permeability contrast values, the lower bed does not contribute to fluid flow and the top layer becomes the only medium of fluid intrusion.

The location of the tip of the concentration profile ()often denoted as fingertip location) is an indication of how a convective cell helps carry a certain species along the direction of flow. The fingertip location (expressed as d/D, where d is the distance of the fingertip from the top surface and D the total thickness of the porous bed) is plotted as a function of the permeability ratio in Fig. 6. Even though the locations of the fingertips are identified only 180 s after the release of the cold water, there is a considerable change in the position. At lower permeability ratio values, the fingertip remains close to the surface (for instance, for permeability ratio of 0.5, the fingertip is only 15% below the surface). Note that gravity does not play any role because the same density of fluid was assumed to be true for this case. The convective term is responsible for dragging the fingertip along the surface of the porous medium. As the permeability ratio increases, the fingertip penetrates deeper into the porous bed. This penetration is linearly proportional to the permeability ratio for a permeability ratio of up to 10 beyond which the fingertip ceases to penetrate any further. At its stable condition, the fingertip penetrates approximately 42% from the surface. Note that the interface between the two-permeability layers is located 50% below the surface.

Contrast=0.5

Contrast=3.0

Contrast=10

Contrast=50

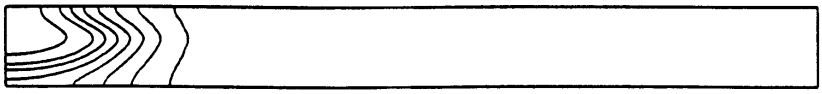

Contrast=100

Fig. 2. Concentration profiles for different permeability contrasts 180 s after the release ($C_{max} = 0.99$, $\Delta C = 0.05$).

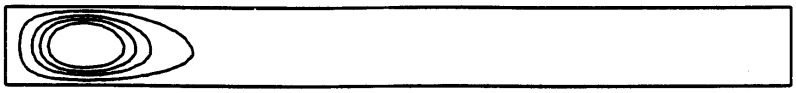

Contrast=0.5

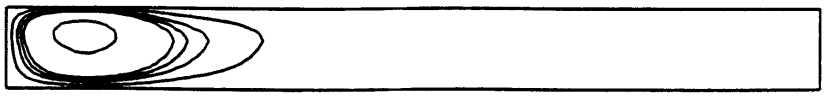

Contrast=3

Contrast=10

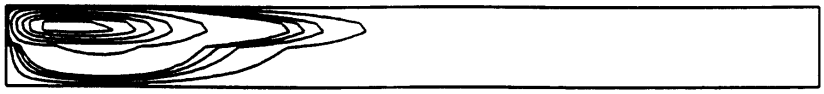

Contrast=50

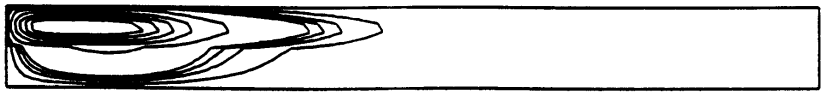

Contrast=100

Fig. 3. Stream function contours for different permeability contrasts 180 s after the release ($\psi_{max} = 0.0015$, $\Delta\psi = 0.0003$).

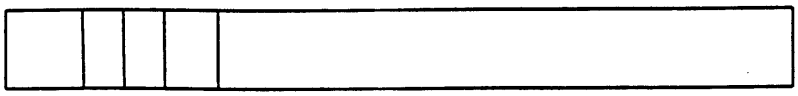

Contrast=0.5

Contrast=3

Contrast=10

Contrast=50

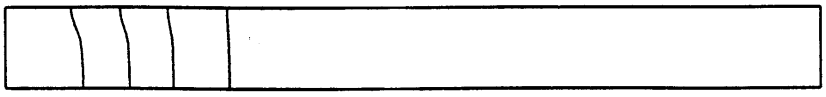

Contrast=100

Fig. 4. Temperature distribution for different permeability contrasts 180 s after the release ($\theta_{max} = 0.95$, $\Delta\theta = 0.05$).

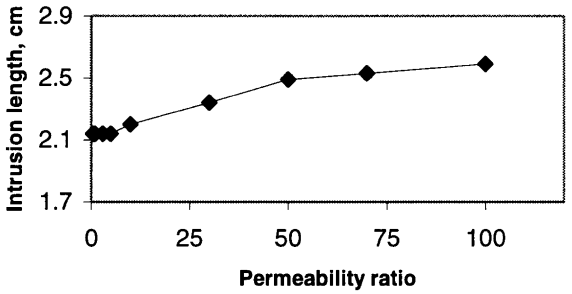

Fig. 5. Intrusion length as a function of permeability ratio 180 s after the release.

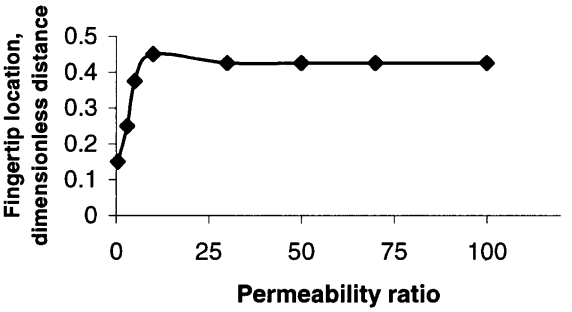

Fig. 6. Fingertip location from the top as a function of permeability ratio 180 s after release.

3.2. Effect of Lewis number

As explained earlier, the Lewis number *Le* is known to be the ratio of the Schmidt number *Sc* to the Prandtl number *Pr*. In this study, the Lewis number, *Le*, was varied in order to observe the relative contribution of thermal diffusivity over solutal diffusivity.

In order to observe the role of Lewis number in determining the propagation of a double diffusive stratified layer, a numerical run using a Lewis number of 100 was conducted for a permeability ratio of 30. This permeability ratio exhibited transition between two stabilized regimes (see Fig. 5) and was considered to be an interesting case for studying the role of both solutal and thermal parameters. For this case, the transient behavior was also observed. Figure 7 shows the intrusion length as a function of time for two cases of Lewis numbers. The dotted line shows the growth in intrusion length for $Le = 1$. Note that the finger propagation rate is nearly constant throughout the propagation for $Le = 1$, especially during the initial stages of the release. There appears to be a slight slowdown in the propagation of the released fluid at a later stage. This effect is much more pronounced for the case of the higher Lewis number. Throughout the period observed, the higher Lewis number case exhibits consistently greater intrusion length.

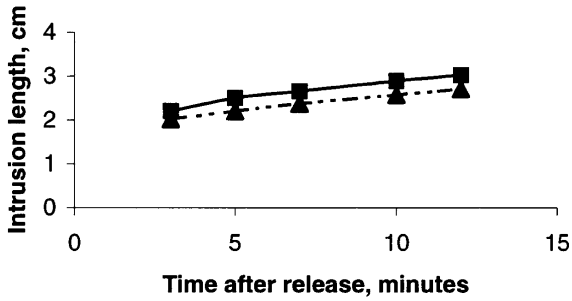

Fig. 7. Intrusion length for two different Lewis numbers (dotted lines: $Le = 1$; solid line: $Le = 100$).

Note that the two lengths remain close to each other at early times (e.g. 3 min). As the time progresses, they quickly diverge to reach a constant difference between them. The transition between these two modes is short-lived. Following the initial period, the two profiles appear to be identical in shape. Even though, the difference in intrusion length appears to be insignificant, the relative difference between the two is not negligible. For instance, within three minutes of the initiation, a higher Lewis number shows 9% increase in intrusion length. At the end, the difference reaches as much as 16%. Considering that the propagation has taken place for a short span of time, this difference is significant. Although, the Lewis number was varied by a factor of 100, the impact being only on the diffusive term (see equation 14), the intrusion length should not be affected beyond what is observed. A higher Lewis number has much more profound impact on the shape of the solutal front [9]. This aspect is discussed in the following paragraphs.

Figure 8 shows the transition of fingertip location for $Le = 1$ for the case of a permeability ratio of 30. For the first 5 min, the fingertip location remains unaltered. Following this initial period, the finger rises toward the surface slightly, only to dip downward afterwards. There is a significant downward movement of the fingertip after 10 min. At the 12 min mark, the finger location enters

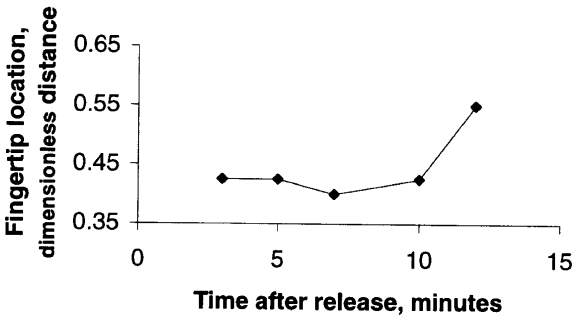

Fig. 8. Distance of the fingertip from the surface ($Le = 1$, permeability ratio = 30).

t=180s

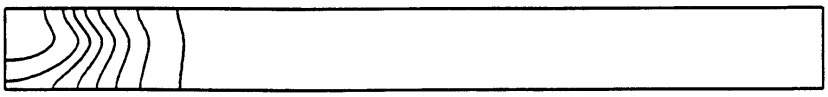

t=300s

t=420s

t=600s

t=720s

Fig. 9. Concentration profiles for $Le = 1$ as a function of time after release ($C_{max} = 0.99$, $\Delta C = 0.05$).

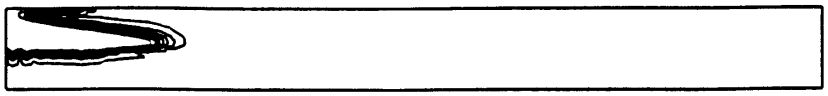

t=180s

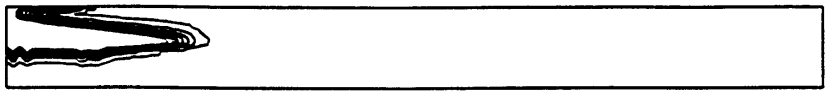

t=300s

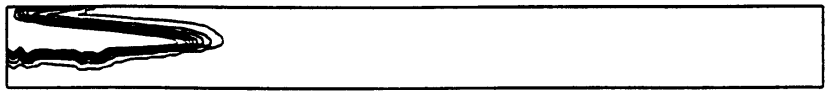

t=420s

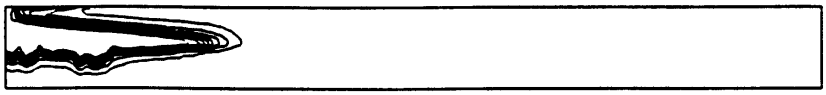

t=600s

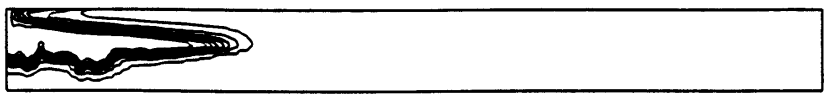

t=720s

Fig. 10. Concentration profiles for $Le = 100$ as a function of time after release ($C_{max} = 0.99$, $\Delta C = 0.05$).

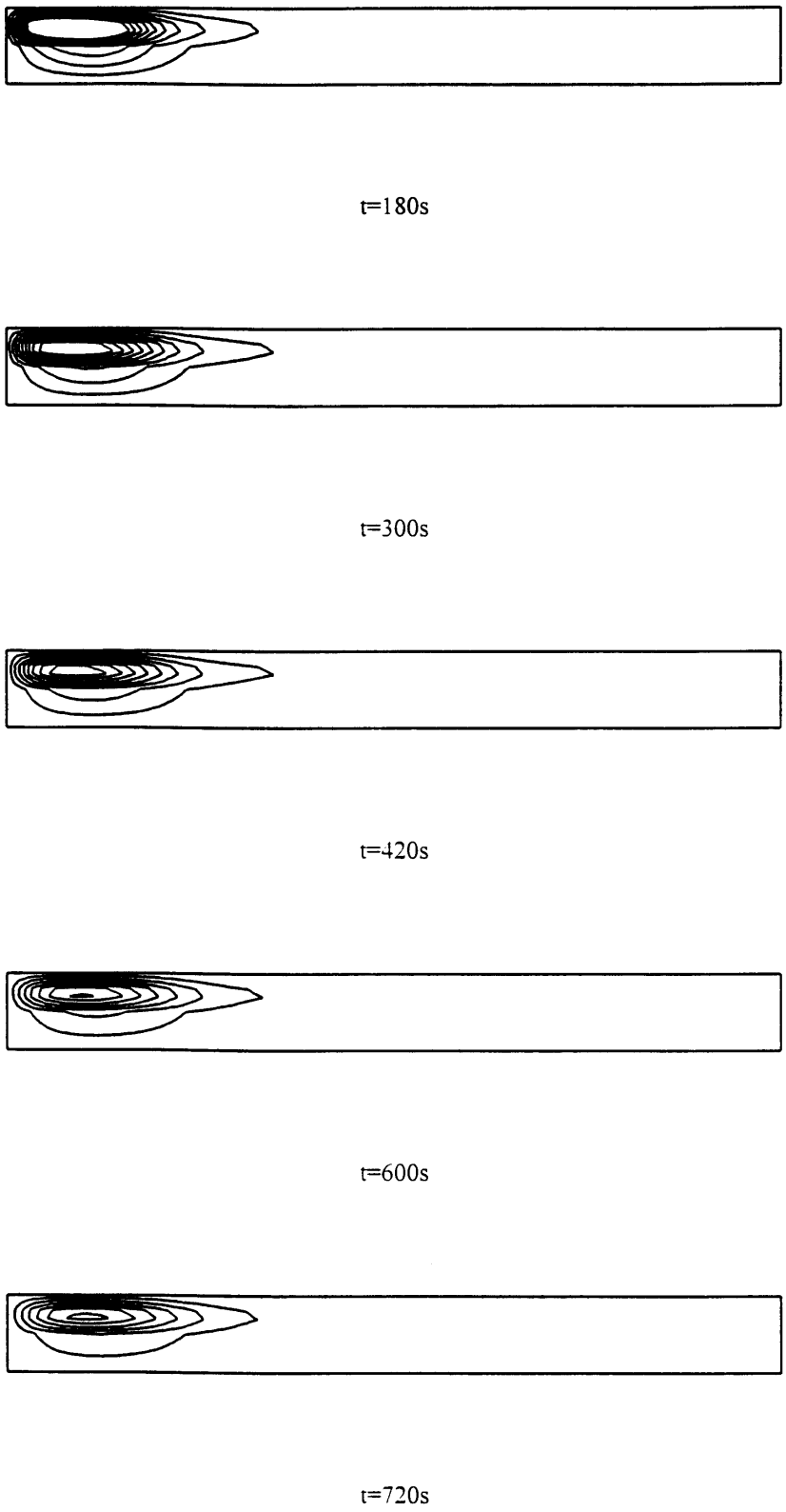

Fig. 11. Stream function for $Le = 1$ as a function of time after release ($\psi_{max} = 0.0009$, $\Delta\psi = 0.0001$).

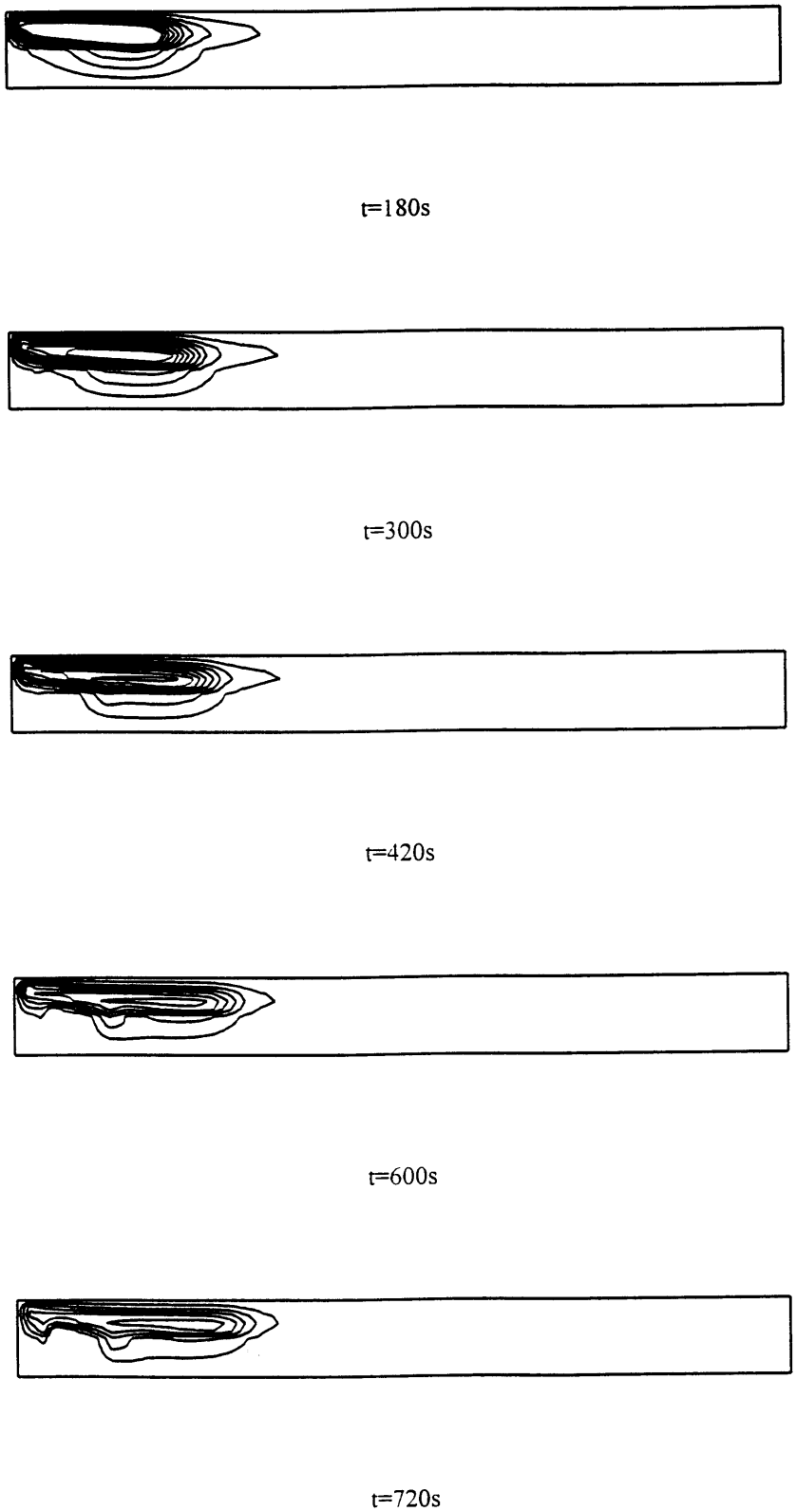

Fig. 12. Stream function for $Le = 100$ as a function of time after release ($\psi_{max} = 0.0009$, $\Delta\psi = 0.0001$).

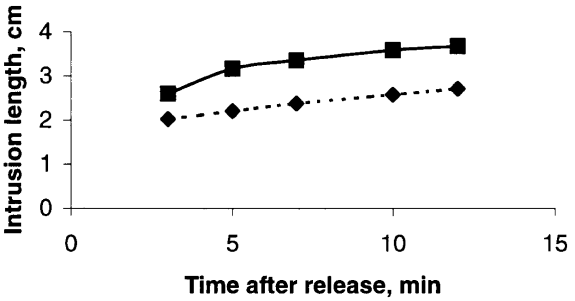

Fig. 13. Effect of temperature difference on intrusion length (dotted line: $\Delta T = 1^{\circ}C$; solid line: $\Delta T = 20^{\circ}C$).

the low-permeability layer for the first time (past the 50% level). The shape of the finger is quite different for Le of 100. For this case, the pointed fingertip remains unusually stable and hovers around 40% below the surface.

Figures 9 and 10 show the transient concentration profiles of $Le = 1$ and $Le = 100$, respectively, for the case of a permeability contrast of 30. They show clearly how greater Le leads to faster propagation of the concentration front. Interestingly, the vertical position of the fingertip (of the concentration profile) remains unusually stable for $Le = 100$. Also, all concentration contours are very compressed for $Le = 100$, showing much greater accumulation in the top part of the formation in which stronger convection was allowed by the presence of a high-permeability layer.

Figures 11 and 12 show transient stream function contours of the same case as described above. The stream function contours do not show nearly as much discrepancy between the two Le cases as did the concentration profiles. At an early stage, both cases show moderate intrusion into the low-permeability layer with similar convective strength in the top layer for both cases. As time progresses, the intrusion front propagates in the shape of a plume and the convection in the lower layer (of low permeability) continues to be weaker. Even though the weakening of convection in the lower layer is apparent for both cases, only the $Le = 100$ case shows the existence of multicellular flow, approximately 10 min after the release of the solution. The emergence of multicellular convection will explain why the concentration front propagates faster in the $Le = 100$ case. However, as multiple cells actually form, there is a blunting of the propagation front. This is evident from the shape of the inner cells in the $Le = 100$ case. Also, because the multicellular pattern only emerges in the top layer, convection in the bottom layer is weakened.

3.3. Effect of thermal contrast

A new numerical run was conducted with a temperature difference of 20°C between the released and the resident fluid. This compares to a temperature difference of 1°C that was used in all previous runs. The permeability ratio was once again set to 30. Note that the same permeability ratio was chosen to investigate the role of Lewis number. Figure 13 shows a comparison of the intrusion length at various times for the two different temperature cases. An increase in the temperature difference accounts for a much faster intrusion rate. A higher rate of propagation is sustained throughout the time period observed. In addition, at a later time, the higher ΔT case gives rise to a reduced degree of cooling, as reflected in the intrusion length. Consequently, the intrusion length curve assumes a shape different from the one observed for the lower thermal contrast case. Figure 14 shows the temperature profiles for the higher thermal contrast case. It is expected that the distance traveled by the temperature contours will be different for the two different cases. However, comparison of temperature contours indicates that the shapes of the curves are also different. Vertical temperature profiles are nonexistent for the higher temperature-contrast case, whereas the lower temperature-contrast case exhibits vertical profiles as early as 7 s after the cold liquid is released. A non-vertical temperature profile is indicative of non-uniform propagation of heat in the two porous layers. At a temperature difference of only 1°C, the thermal convection is so weak that the effect of permeability contrast is not reflected in the temperature profile.

Propagation of the thermal fronts for both 1 and 20°C are plotted in Fig. 15. This figure shows that the higher ΔT case was only slightly different than the lower ΔT case at the early times. However, as the time progresses, the thermal front travels much faster for the higher ΔT case. Note that the temperature difference was imposed only during the release of the cold fluid. When Fig. 15 is compared with Fig. 13, it is clearly seen that the thermal front travels faster than the concentration front. Even though the Lewis number was set equal to unity for these cases (equal thermal and solutal diffusion), the mass balance equation does not collapse to the same form as the energy balance equation continues to yield concentrations that are different from the temperatures of the same case.

4. Conclusions

Double diffusive convection in porous medium is studied in the context of multi-layered porous media. Both solutal and thermal convective cells were considerably weakened in the low-permeability zone, but only after the permeability contrast become more than 10-fold. The intrusion length was affected significantly by an increase in the permeability ratio of the two layers. However, for a permeability ratio beyond 50, convection in the low-permeability layer became so weak that the intrusion

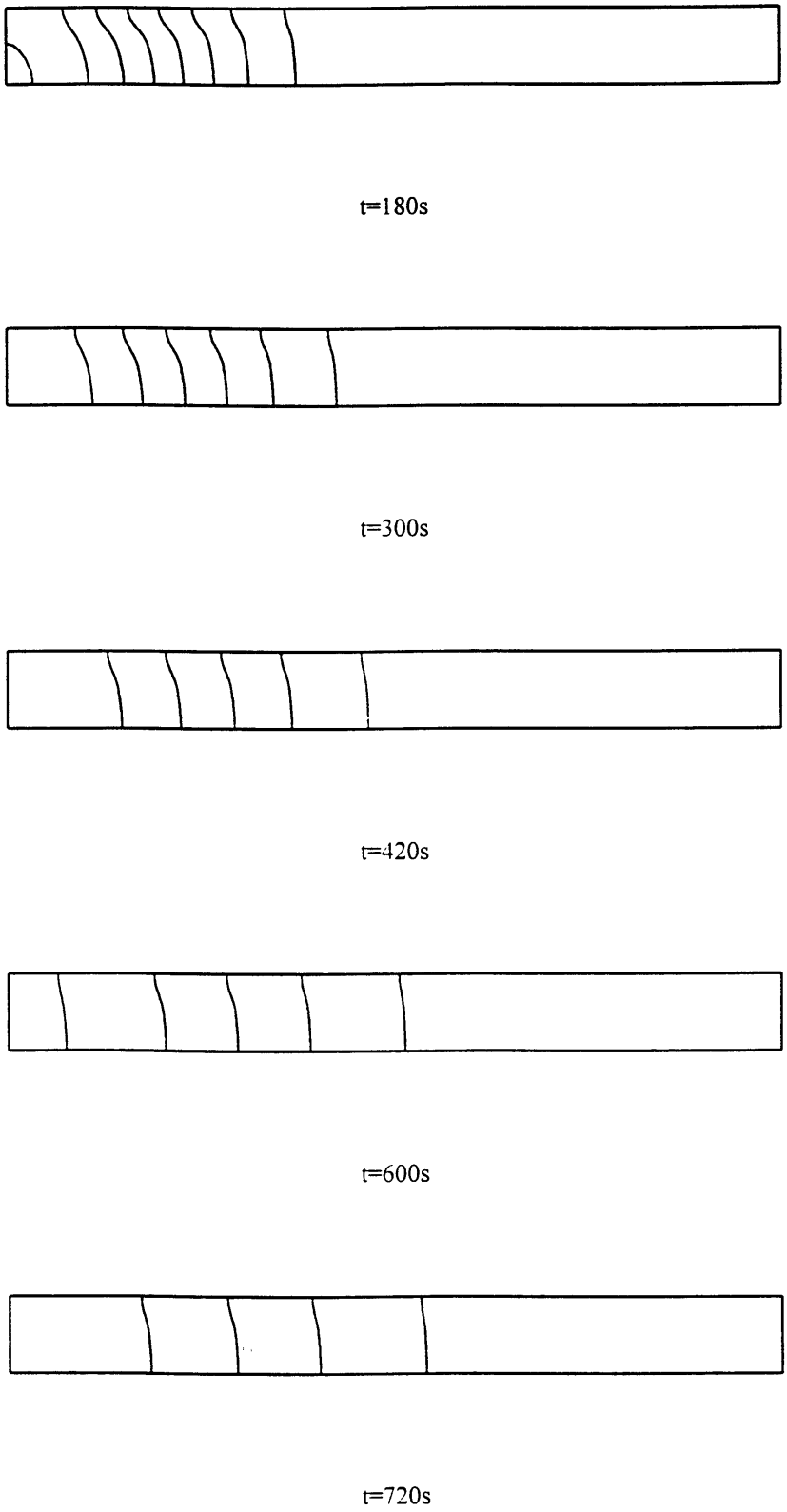

Fig. 14. Transient temperature contours for a temperature difference of $\Delta T = 20^{\circ}C$ and $Le = 1$ ($\theta_{max} = 20$, $\Delta\theta = 0.5$).

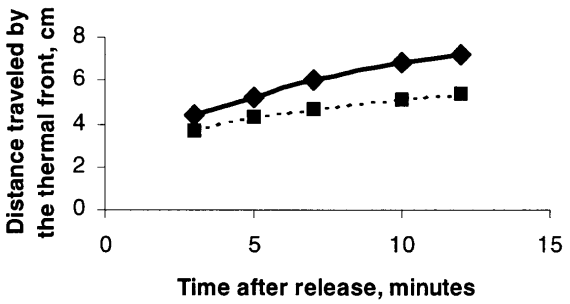

Fig. 15. Propagation of the thermal front (dotted line: $\Delta T = 1^{\circ}C$; solid line: $\Delta T = 20^{\circ}C$).

length became insensitive to higher permeability ratios. Even though the permeability discontinuity was placed at the 50% height, the center of the solutal front (called the fingertip) remained in the upper layer. However, the location of the fingertip remained a strong function of the permeability contrast for a permeability contrast below 50. Also, it was found to be time dependent.

Lewis number plays a role in determining the intrusion length, with increasing intrusion length as the Lewis number was increased. However, no time dependence was observed beyond the initial few minutes of cold water release. For the higher Lewis number case, multicellular convection was observed following initial unicellular flow. The emergence of multicellular convection was attributed to the presence of a dual-permeability system with stronger convection in the higher-permeability zone.

The temperature contrast between the injected cold water and the resident warm water had a significant impact on both intrusion length and the propagation of the thermal front. The propagation of the thermal front, however, appeared to be more transitory in nature than was the intrusion length. Permeability contrast, in itself, played a greater role in the presence of a higher temperature difference between the two fluids.

In general, the variation of permeability in a porous layer affects all governing parameters of heat and mass transport. However, the intensity of these effects is greater beyond a certain permeability contrast. Also, most of the phenomena observed became insensitive to the permeability ratio as the permeability ratio reached a high value at which point convection (both thermal and solutal) remained confined to be higher-permeability zone.

Acknowledgements

The authors would like to acknowledge the financial support of the Zayed International Agricultural and Environmental Research Program and the Abu-Dhabi National Oil Company (ADNOC).

References

[1] J. Yoshida, H. Nagashima, M. Nagasaka, A double diffusive lock-exchange flow with small density difference, Fluid Dynamics Res. 2 (1987) 205–215.
[2] R.W. Schmitt, Why didn't Rayleigh discover salt fingers? Double Diffusive Convection Geophysical Monograph 94 (1994) 3–10.
[3] T. Maxworthy, The dynamics of double diffusive gravity currents, J. Fluid Mech. 128 (1983) 259–282.
[4] M.Z. Saghir, M. Hennenberg, M.R. Islam, Double diffusive convection with Marangoni effects in a multi-cavity system, Int. J. Heat and Mass Transfer 41 (14) (1998) 2157–2174.
[5] D.A. Nield, A. Bejan, Convection in Porous Media. Springer-Verlag, 1992.
[6] D.M. Manole, J.L. Lage, D.A. Nield, Convection induced by inclined thermal and solutal gradients with horizontal mass flow, in a shallow horizontal layer of a porous medium, Int. J. Heat Mass Transfer 37 (14) (1994) 2047–2057.
[7] F. Chen, C.F. Chen, Double-diffusive fingering convection in a porous medium, Int. J. Heat Mass Transfer 36 (3) (1993) 793–807.
[8] Z. Zongqin, A. Bejan, The horizontal spreading of thermal and chemical deposits in a porous medium, Int. J. of Heat and Mass Transfer 30 (11) (1987) 2289–2303.
[9] A. Basu, M.R. Islam, Instability in a combined heat and mass transfer problem in porous media, Chaos, Solit. and Frac. 7 (1) (1996) 109–123.
[10] M.Z. Saghir, Heat and mass transfer in multi-porous cavity, Int. Comm. Heat and Mass Transfer, accepted.
[11] M.R. Islam, K. Nandakumar, Transient convection in saturated porous layers with internal heat sources, Int. J. Heat and Mass Transfer 33 (1) (1990) 151–161.
[12] J. Carter, M.R. Islam, Thermal and concentration induced instability in porous media. Proceedings of 9th Nuclear Thermal Hydraulics, Winter Meeting, San Francisco, U.S.A., 1993, pp. 157–67.
[13] K.J. Weber, How Heterogeneity Affects Oil Recovery. Reservoir Characterization. Academic Press, U.S.A., 1986.
[14] A. Ahmadi, A. Lastie, M. Quintard, Large-scale properties for flow through a stratified medium: various approaches. SPE Res. Eng., 1993 pp. 214–220.
[15] T.J. Lasseter, J.R. Waggoner, L.W. Lake, L.W. Lake, Reservoir Heterogeneities and Their Influence on Ultimate Recovery. Reservoir Characterization, Academic Press, U.S.A., 1986.
[16] M.M. Honarpour, A.S. Cullick, N. Saad, N.V. Humphreys, Effect of rock heterogeneity on relative permeability: Implication for scaleup. SPE 29311: Proceedings of 1995 SPE Asia Pacific Oil Gas Conf. Kuala Lumpur, Malaysia, 20–22 March, 1995.
[17] P.S. Ringrose, K.S. Sorbe, P.W. Corbett, J.L. Jensen, Immiscible flow behaviour in laminated and cross-bedded sandstone, J. Pet. Sci. Eng. 9 (1993) 103–124.
[18] T. Eilertsen, K.A. Borresen, H. Bertin, A. Graue, Experiments and numerical simulation of fluid flow in a cross-layered reservoir model, J. Pet. Eng. Sci. 18 (1997) 49–60.
[19] P. Ingsoy, R. Gauchet, L.W. Lake, Pseudofunction and extended Dietz theory for gravity-segregated displacement in stratified reservoirs. SPE Reservoir Eng. Feb. 67–72, 1994.

[20] G. Ahmed, L.M. Castanier, W.E. Brigham, An experimental study of waterflooding from a two-dimensional layered sand model, SPE Reservoir Eng. 3 (1) (1988) 45–54.
[21] H. Bertin, M. Quintard, P.V. Corpel, S. Whitaker, Two-phase flow in heterogeneous porous media III: laboratory experiments for flow parallel to a stratified system, Transp. Porous Media 5 (1990) 543–590.
[22] W. Alhanai, H. Bertin, M. Quintard, Two-phase-flow in modular systems: laboratory experiments, Rev. Inst. Frac. Pet. 47 (1) (1992) 29–44.
[23] H. Bertin, W. Alhanai, A. Ahmadi, M. Quintard, Two-phase flow in heterogenous nodular porous media, in P.F. Worthington, C. Chardaire-Riviere (Eds.), Advances in Core Evaluation, vol. III, 1993, pp. 471–487.
[24] H.A. Tchelepi, F.M. Orr, Jr., Interaction of viscous fingering permeability heterogeneity, and gravity segregation in three dimensions, SPE Reservoir Eng., 1994, Nov. 266–271.
[25] W.B. Zimmerman, G.M. Homsy, Three-dimensional viscous fingering: a numerical study, Phys. Fluids A, 4 (1992) 1901.
[26] M.A. Combarnous, S. Bories, Hydrothermal convection in a saturated porous media, Advances in Hydroscience 10 (1975) 231–305.
[27] M.R. Islam, K. Nandakumar. Multiple solution for buoyancy-induced flow in saturated porous media for large Peclet numbers, Trans. ASME J. of Heat Transfer 108 (4) (1986) 866–871.
[28] M.R. Islam, Mixed convection in a large-aspect ratio porous medium under non-Darcy flow regime. Mixed Convection Heat Transfer. HTD-247, ASME (1993) 79–86.